

A New Hydrophilic Binder Enabling Strongly Anchoring Polysulfides for High-Performance Sulfur Electrodes in Lithium-Sulfur Battery

Wei Chen, Tianyu Lei, Tao Qian, Weiqiang Lv, Weidong He,* Chunyang Wu, Xuejun Liu, Jie Liu, Bo Chen, Chenglin Yan,* and Jie Xiong*

As one of the important ingredients in lithium-sulfur battery, the binders greatly impact the battery performance. However, conventional binders have intrinsic drawbacks such as poor capability of absorbing hydrophilic lithium polysulfides, resulting in severe capacity decay. This study reports a new type of binder by polymerization of hydrophilic poly(ethylene glycol) diglycidyl ether with polyethylenimine, which enables strongly anchoring polysulfides for high-performance lithium sulfur batteries, demonstrating remarkable improvement in both mechanical performance for standing up to 100 g weight and an excellent capacity retention of 72% over 400 cycles at 1.5 C. Importantly, in situ micro-Raman investigation verifies the effectively reduced polysulfides shuttling from sulfur cathode to lithium anode, which shows the greatly suppressed shuttle effect by the polar-functional binder. X-ray photoelectron spectroscopy analysis into the discharge intermediates upon battery cycling reveals that the hydrophilic binder endows the sulfur electrodes with multidimensional Li-O, Li-N, and S-O interactions with sulfur species to effectively mitigate lithium polysulfide dissolution, which is theoretically confirmed by density-functional theory calculations.

a value of 1675 mA h g⁻¹ or 2800 Wh L⁻¹ on weight or volume basis, respectively. With over fivefold energy capacity, sulfur demonstrates superior advantages over current commercial intercalation compound (LiCoO₂ and LiFePO₄) cathode materials.^[3–5] Despite its considerable advantages, the practical application of Li-S battery has been hindered by poor cycle life due to the shuttle effect, leading to quick capacity decay due to the loss of active materials and an low Coulombic efficiency.^[6,7] Moreover, the insulating nature of S/Li₂S and as large as 78% volume expansion of sulfur cathode when initial state S (2.03 g cm⁻³) is fully converted to final state Li₂S (1.66 g cm⁻³) result in rapid capacity fading and short cycle life due to the low utilization of active materials and poor electrical contact between sulfur particles and conductive additives.^[8,9] Aiming to address these

Lithium-ion batteries (LIBs) with high energy density have been applied in a variety of energy storage devices to address the increasing energy storage demands for various technological applications, including portable electronic devices, electric vehicles, and hybrid electric vehicles.^[1,2] Among LIBs, lithium-sulfur (Li-S) battery has received tremendous attention arising from the exceptional theoretical capacity of sulfur with

negative impact of at least some of the detrimental processes described above for realizing commercial application of high-energy Li-S battery, various considerable strategies have been focused on cathode material modification including N-doped materials,^[10–12] porous materials,^[13] hierarchical materials,^[14] metal oxides^[15,16] transition metal disulfides,^[17] and functional separator modification,^[18,19] as well as employment of solid or


W. Chen, T. Lei, C. Wu, Prof. J. Xiong
State Key Laboratory of Electronic Thin Film and Integrated Devices
University of Electronic Science and Technology of China
Chengdu 610054, China
E-mail: jixiong@uestc.edu.cn

Dr. T. Qian, X. Liu, J. Liu, Prof. C. Yan
Soochow Institute for Energy and Materials Innovations
College of Physics
Optoelectronics and Energy & Collaborative Innovation Center
of Suzhou Nano Science and Technology
Soochow University
Suzhou 215006, China
E-mail: c.yan@suda.edu.cn

Dr. T. Qian, X. Liu, J. Liu, Prof. C. Yan
Key Laboratory of Advanced Carbon Materials and Wearable Energy
Technologies of Jiangsu Province
Soochow University
Suzhou 215006, China

Dr. W. Lv, Prof. W. He
School of Energy Science and Engineering
University of Electronic Science and Technology of China
Chengdu 610054, China
E-mail: weidong.he@uestc.edu.cn

Dr. B. Chen
Institute of Microelectronics of Chinese Academy of Sciences
Beijing 100029, China

 The ORCID identification number(s) for the author(s) of this article can be found under <https://doi.org/10.1002/aenm.201702889>.

DOI: 10.1002/aenm.201702889

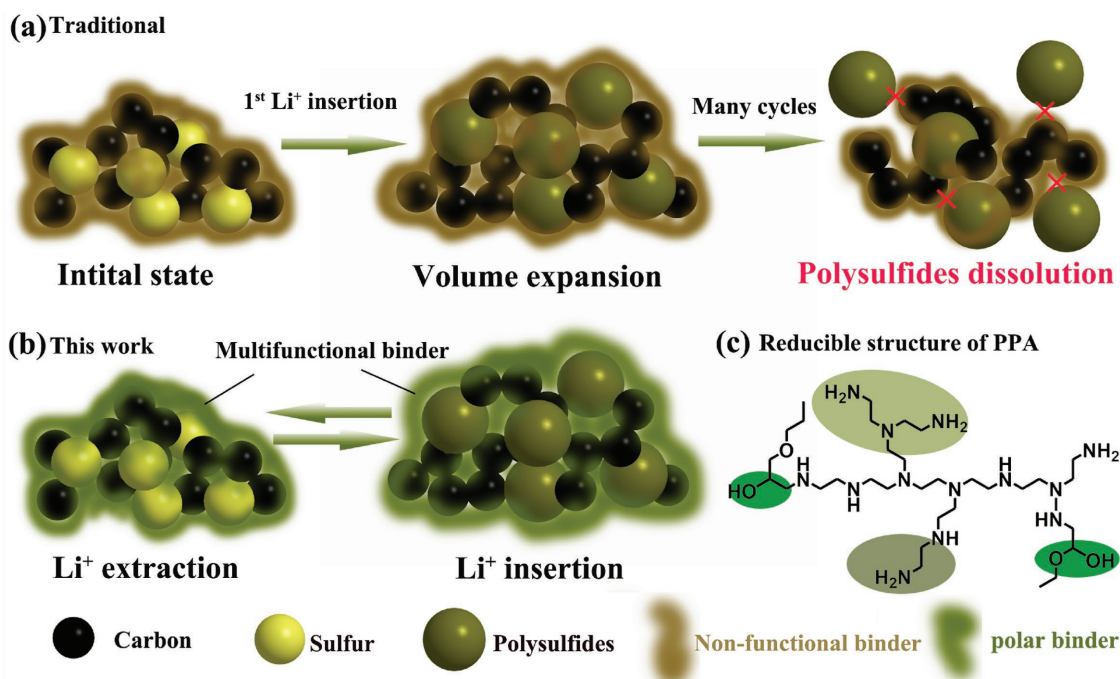


Figure 1. Schematics of the binder: a) Traditional approaches to maintain electrode construction using PVDF as mechanical binder indicating that intermediate sulfur species fast dissolve with time. b) Polar polymer with abundant amino and amide groups. c) The reducible molecular structure of multiactive sites binder of PPA for tailoring chemical and physical ability for improving the performance of the Li-S battery.

quasi-solid electrolytes.^[20–22] Those tremendous efforts have achieved benefited ability to circumvent polysulfide dissolution and the shuttle effect for achieving significant improvements in specific capacity, cycling stability, and cycle life of Li-S batteries.

The binder as an important component in lithium battery to stabilize the electrode is highly important. However, the binder has been rarely investigated and attracted less attention in the Li-S battery field. Poly(vinylidene fluoride) (PVDF) as a conventional binder has been widely used in traditional Li-S batteries due to the acceptable adhesion and wide electrochemical window.^[23,24] However, the nonfunctionalized chain structure of the PVDF binder cannot afford sufficient binding to polysulfides, and the shuttling effect still occurs (Figure 1a).^[25] In contrast, the functionalizing polymer binders with additional chemical bonds to anchor polysulfides are a well-known strategy for stabilizing the sulfur cathode because irreversible dissolution of polysulfides is mitigated (Figure 1b).^[26–30] For instance, Zhang and co-workers employed gum arabic as bifunctional binder that shows strong chemical bonding between both sulfur and polysulfides,^[26] resulting in the long cycle life of 500 cycles with a capacity retention of 72.7% at 0.5 C. Xiao and co-workers developed a functional binder (poly-amidoamine dendrimers) with high degree of surface functionalities, interior porosities, and polarity, which allows for high S loadings (>4 mg cm⁻²) in Li-S batteries.^[27] Very recently, the authors demonstrated that the polar binder (AFG) could perfectly trap polysulfides and maintain electrode integrity.^[30] However, it has been found that the AFG binder is not dissolved with most of the solvents such as water, ethanol, acetone, acetonitrile, *N*-methyl-2-pyrrolidone, and dimethyl formamide (DMF) that resulting the AFG binder has to be dispersed

with micropartials and then be used (Figure S3, Supporting Information).

To address the aforementioned issues, herein we propose a new hydrophilic binder with strong adhesion performance and abundant polar groups, which could effectively advance the Li-S battery toward commercialization. As shown in Figure 1c, on the basis of this conceptual motivation, poly(ethylene glycol) diglycidyl ether (PEGDGE) is used to crosslink polyethylenimine (e-PEI) to form hyperbranched binder (denoted as PPA binder; Figures S1 and S2, Supporting Information). Thus, the high polar affinity and strong binding characteristics of PPA binder can strongly trap polysulfides. Furthermore, in situ micro-Raman investigation clearly reveals that the dissolution of polysulfides is effectively suppressed because only weak mid-chain Li₂S₄ Raman signal is detected. In addition, the strong affinity energy of polysulfides to PPA binder is verified by density-functional theory (DFT) calculations, which yields the substantial Li–O and Li–N bonding.

Fourier transform infrared spectroscopy (FTIR; Figure S4, Supporting Information) and X-ray photoelectron spectroscopy (XPS; Figure S5, Supporting Information) survey scanning spectra are utilized to analyze the chemical structure of the covalently cross-linked PPA binder (Figure S2, Supporting Information). As presented in Figure S4 (Supporting Information), prior to cross-linking reaction, a relatively strong peak at ≈3400 cm⁻¹ is observed, which corresponds to the characteristic peaks of the stretching vibration of the secondary amine groups. In addition, the weak peaks at 1668–1300 cm⁻¹ are observed for the pristine PEI sample, which is assigned to the NH₂ bending vibration of primary amine on the frame construction of PEI. For PEGDGE, the observed peak at 2900 is

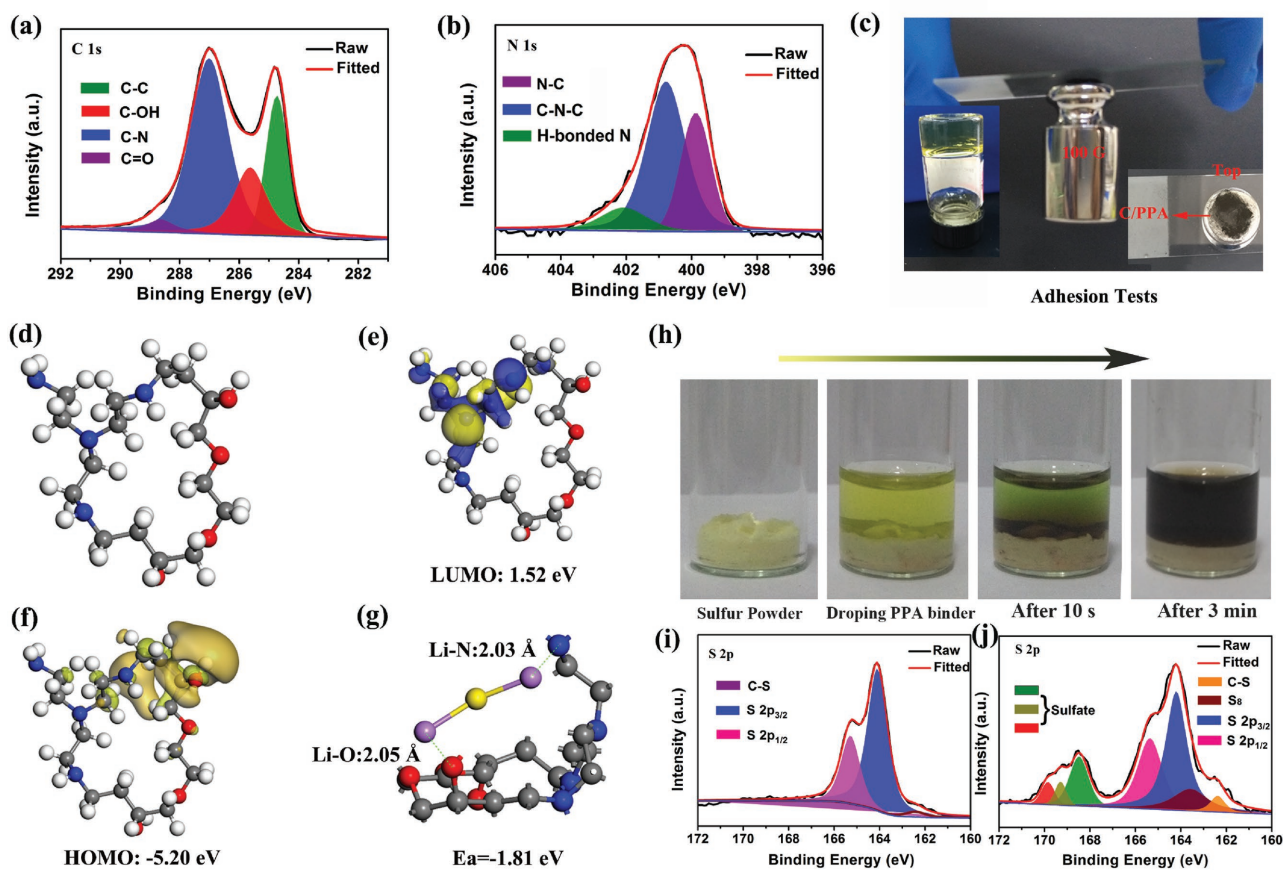


Figure 2. Characterization of multifunctional binder PPA. a,b) High-resolution XPS of C1s and N1s spectra of PPA, respectively. c) Schematic representation of the setup used to perform the adhesion tests for the PPA binder, and the inset digital image shows the vials with the PPA binder after DMF evaporation. d) Structure of reducible PPA binder deduced from DFT analysis. Calculated band structures of e) LUMO and f) HOMO for evaluating PPA electrochemical window. g) Calculated binding energy between PPA and Li_2S , showing strong Li–O and Li–N bond. h) Digital images of shown chemical bonding test of PPA binder with sulfur. i,j) The high-resolution XPS analyses of S 2p before and after exposing to the PPA binder, respectively.

attributed to the stretching vibration of the epoxy group.^[31] After the indiscriminating reactions, the FTIR results of the PPA binder indicate that the bond of epoxy group at 2900 cm^{-1} gradually disappears, confirming the bonding between PEI and PEGDGE occurred. Excessive amine groups remain available for interaction with polysulfides even after cross-linking reaction. These results are further verified by XPS scanning spectra, as presented in **Figure 2a,b**. Deconvolution of the C 1s signal can be well resolved into three peaks corresponding to C–N amine bond at 287.2 eV, C–O hydroxyl bonding at 285.7 eV, and C–C bonding at 284.7 eV. Besides the C signal, the N 1s signals are from both amine (399.7 eV) and amide (401.5 eV) groups. It implies that amino groups are retained after reaction, which is consistent with FTIR results. Furthermore, the C–O–H (533.6 eV) 1s peak from PPA appears in the wide O 1s spectra (Figure S5, Supporting Information), indicating that PEI has taken part in the reaction with PEGDGE. Besides structure characterization of PPA binder, adhesion tests are further conducted to qualitatively evaluate and compare the mechanical property of the PPA binder. As shown in **Figure 2c**, the results indicate that the PPA polymer could afford strong mechanical strength as high as 100 g weight, whereas PVDF cannot support any mass weight. The adhesion tests clearly demonstrate

that the robust bond of PPA binder chains contributes to the mechanical strength after cross-linking reaction between PEI and PEGDGE.^[32] Clearly, these results imply that the strength of the whole electrode is greatly improved with PPA binder, which can help to buffer the volume changes during the cycling process, preventing active material from exfoliation and maintaining the integrity of the electrode, especially under the long-term cycling conditions.

Wide electrochemical windows of binders are undoubtedly important for Li-S batteries because the high chemical potential of sulfur cathodes ($\approx 3\text{ V}$) has the ability to decrease the electrochemical stability and even destroy the structure of binder in the cathode if the highest occupied molecular orbital (HOMO) of the binder is larger than -4.46 eV (the conversion relationship between V and eV is described in the Experimental Section).^[29] Therefore, Gaussian calculations are employed to analyze the band structure of PPA binder to evaluate the electrochemical window of PPA binder.^[33] As shown in **Figure 2e,f**, the calculated results indicate that the PPA binder has a wide energy gap window of $E_g \approx 6.72\text{ eV}$ (the difference between low unoccupied molecular orbital (LUMO) and HOMO) and the HOMO as low as -5.20 eV that is far below -4.46 eV , implying the PPA binder owns not only strong physical bonding strength but also

excellent electrochemical stability in the electrolyte. We further evaluate the chemical adsorption capacity of the PPA binder for polysulfides (elected: Li_2S) by DFT analysis (Figure 2g). Perfect interaction with Li_2S by forming Li–O and Li–N bonds is verified by the strong adsorption energy of 1.81 eV, which provided the strong evidence that PPA binder is suitable for high-energy Li–S battery for anchoring polysulfides. As shown in Figure 2h, we simulate sample preparation processes by simply mixing PPA and S at room temperature to monitor the S atom bond evolution and study the possible chemical bonding between PPA and S. It is surprisingly found that only after 10 s the color at the interface between S and PPA turns fast from light yellow to brown, and the color of the upper liquid changes to the olive, indicating strong chemical bonding occurred between S and PPA binder. We then employ XPS S 2p spectrum (Figure 2i,g) to study the possible chemical bond formation between S and PPA binder, and the results show that strong S–O bond forms as the sulfate signal appears, implying that the chemical bonds are generated between the functional groups of PPA and sulfur powders, which is beneficial for the immobilization of S on nonpolar carbon surface for better ion kinetics.^[26]

We employ commercial sulfur powders to investigate the electrochemical performance of sulfur electrode with PPA binder (Figure S6, Supporting Information). Figure 3a shows the cyclic voltammogram of the S/C/PPA composite cathode at a scan rate of 0.01 mV s^{-1} between 1.5 and 3 V (vs Li/Li^+) for the initial five cycles. Slight polarization is observed in the first activation cycle, which is likely due to the strong adsorption ability of the hybrid carbon matrix.^[34,35] From the second cycle onward, no obvious changes are observed for the sharp redox peaks compared with PVDF binder (Figure S7, Supporting Information), implying that the cathode exhibits good electrochemical stability. According to the multiple reaction mechanism

between S and Li ,^[9] two cathodic peaks are observed: one is located at $\approx 2.3 \text{ V}$ due to the transformation of S_8 to long-chain Li_2S_n ($4 \leq n \leq 8$), and the other at $\approx 2.05 \text{ V}$ is attributed to the further reduction to low-order Li_2S_n ($n < 4$), and finally to Li_2S . The overlapping anodic peaks at $\approx 2.4 \text{ V}$ are caused by the transformation of sulfur species to Li_2S_n ($n > 2$) corresponding to its reverse process. Figure S8 (Supporting Information) shows the typical two-plateau charge/discharge profile of the S/C/PPA composite cathode at the 1st, 2nd, 10th, and 100th cycles at a current rate of 0.5 C ($1 \text{ C} = 1675 \text{ mA g}^{-1}$), which could be assigned to the formation of long-chain polysulfides (high plateau) and short-chain polysulfides (low flat plateau). Compared with PVDF binder (Figure S9, Supporting Information), these plateau patterns remain almost unchanged even after 100 cycles, indicating the excellent electrochemical stability of the S/C/PPA composite cathode.

As depicted in Figure 3b, we comparatively confirm the effects of the PPA binder with different molar fractions of epoxy groups and amine groups on the electrochemical performance of the composite cathode named as $\text{PPA}_{1:2}$, $\text{PPA}_{1:1}$, and $\text{PPA}_{1.5:1}$ over 100 cycles. It could be clearly found that both cycle life and specific capacity are enhanced after PVDF has been replaced with PPA binder. The observed capacity decay at the initial cycles is speculated to be associated with the dynamic balance environment in the Li–S system and the further formation process of solid electrolyte interphase (SEI) layer on the surface of the lithium metal during the initial cycling process. After cycling over ten cycles, the stable capacity retention of PPA binder is achieved. In particular, when the molar fractions of epoxy groups and amine groups are 1:2, a capacity retention of 93% (763 mA h g^{-1}) is achieved at 100 cycles (Figure 3c), which suggests a very small capacity loss of 0.48 mA h g^{-1} per cycle, as calculated based on the tenth cycle at 0.5 C in Figure 3b. Rate

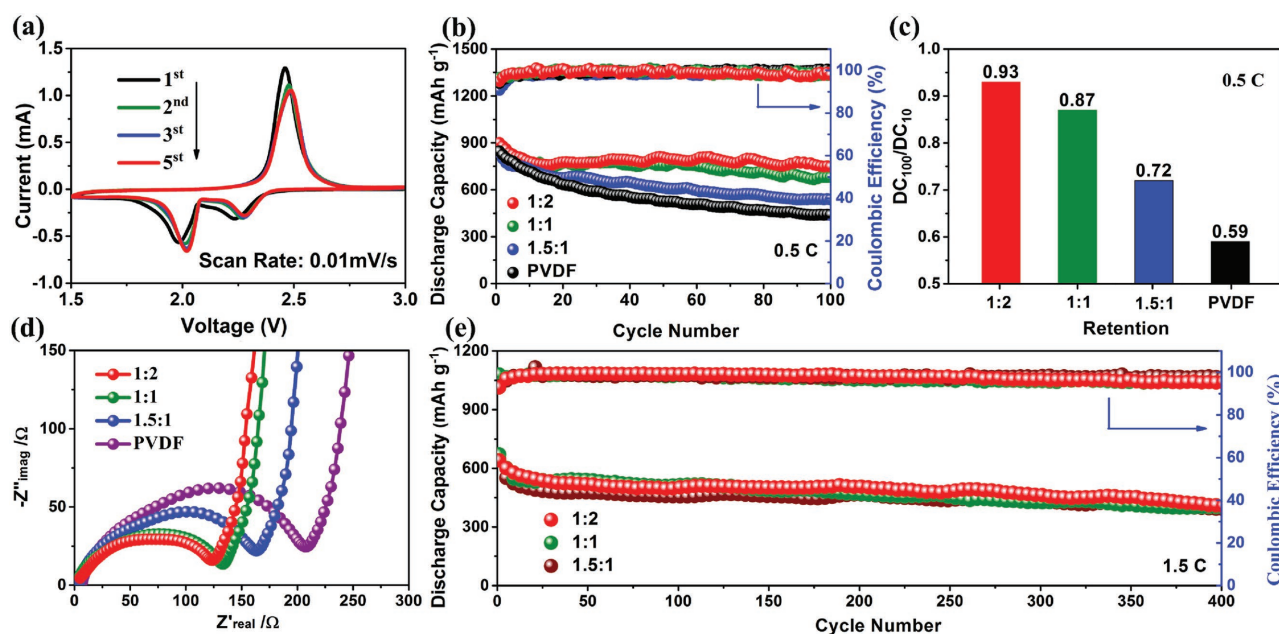


Figure 3. a) Cyclic voltammogram at a scan rate of 0.01 mV s^{-1} . b) Cycling performance and Coulombic efficiency. c) Capacity retention based on the capacity of the tenth cycle in (b). d) Nyquist plot curves of PPA binder and PVDF binder, respectively. e) Long-term cyclability of the cathode with PPA binder with different cross-linked degrees at 1.5 C over 400 cycles.

capabilities of the PPA binder are further investigated as shown in Figure S10 (Supporting Information). The S/PPA_{1,2}, S/PPA_{1,1}, and S/PPA_{1,5,1} electrodes exhibit significantly higher rate capabilities than S/PVDF, especially for the S/PPA_{1,2} and S/PPA_{1,1} electrodes with more amino groups. The significant enhancement in the rate performance of the S/C cathodes should be attributed to the high chemical/mechanical properties of the binder. The advantages of PPA_{1,2} are further confirmed by the electrochemical impedance spectroscopy measurements of PPA and PVDF binder, as conducted within the frequency range between 0.1 Hz and 1 MHz. The Nyquist plots presented shown in Figure 3d are composed of a depressed semicircle at high frequencies corresponding to the solution resistance (R_s) and the interfacial charge transfer resistance (R_{ct}) that is related to the electrochemical activities of the composites.^[35] It is clear that R_{ct} dramatically increases with cross-linking degrees of PPA binder caused by the increased molecular structure that tends to be in an insulating gel state. As comparison, there is a remarkably increased resistance for PVDF. Whereas, after prolonged cycling, the capacity retention of $\approx 72\%$ (from 600 to 430 mA h g⁻¹) at a current density of 1.5 C is obtained (Figure 3e) with cross-linking degree of 1:2 over 400 cycles. Apparently, the enhanced reversibility of PPA_{1,2} binder is attributed to more amino/amide groups, which more efficiently inhibit the leakage of polysulfide.

To re-evaluate the effect of the PPA binder, the LiNO₃ is completely removed from the electrolyte, as shown in Figure S11 (Supporting Information). Both cycling behavior and Coulombic efficiency were significantly increased of PPA binder, and 83.9% capacity retention (Figure S11, Supporting Information) and 90.1% initial efficiency can be obtained after 50 cycles at 1 C.

For comparison, The PVDF binder shows more serious capacity decrease (52.8%) and lower initial efficiency (76.3%). These tests provide a direct demonstration that the PPA binder has effectively capacity to suppress “shuttle effect” and improve both the cycle and Coulomb efficiency compared to PVDF binder. Furthermore, we increased the high sulfur loading with 5.3 mg cm⁻² at 0.2 C for S/C/PPA electrodes (Figure S12, Supporting Information). The stable capacity could be sufficiently obtained, indicating effective capacity of PPA binder for challenging high energy density. Therefore, compared with other traditional binders (such as PVDF, polyvinyl pyrrolidone (PVP), polytetrafluoroethylene (PTFE), and carboxymethylcellulose (CMC)), the PPA binder shows that it can more effectively promote the stable performance of S electrodes (Table S1, Supporting Information), thus making it possible that PPA binder can be easily integrated into other optimized devices by simply replacing the traditional binder with the newly designed binder without modifying the complicated electrode structure, and thus may readily be integrated with other development in field and implemented for practical technologies.

To gain insight into the shuttling mechanism of the polysulfides, in situ micro-Raman spectroscopy is performed by analyzing the evolution of various lithium polysulfides,^[36,37] which is shown in Figure 4a,b. Typically, long and mid-chain polysulfides can be qualitatively determined and clearly distinguished with in situ Raman spectroscopy according to the reaction time and the typical two-plateau voltage profile. As presented in Figure 4c,d, during the discharge process, it is clearly revealed that various long-chain and mid-chain polysulfides are found for the PVDF binder from the time-resolved Raman image, as highlighted according to the theoretical

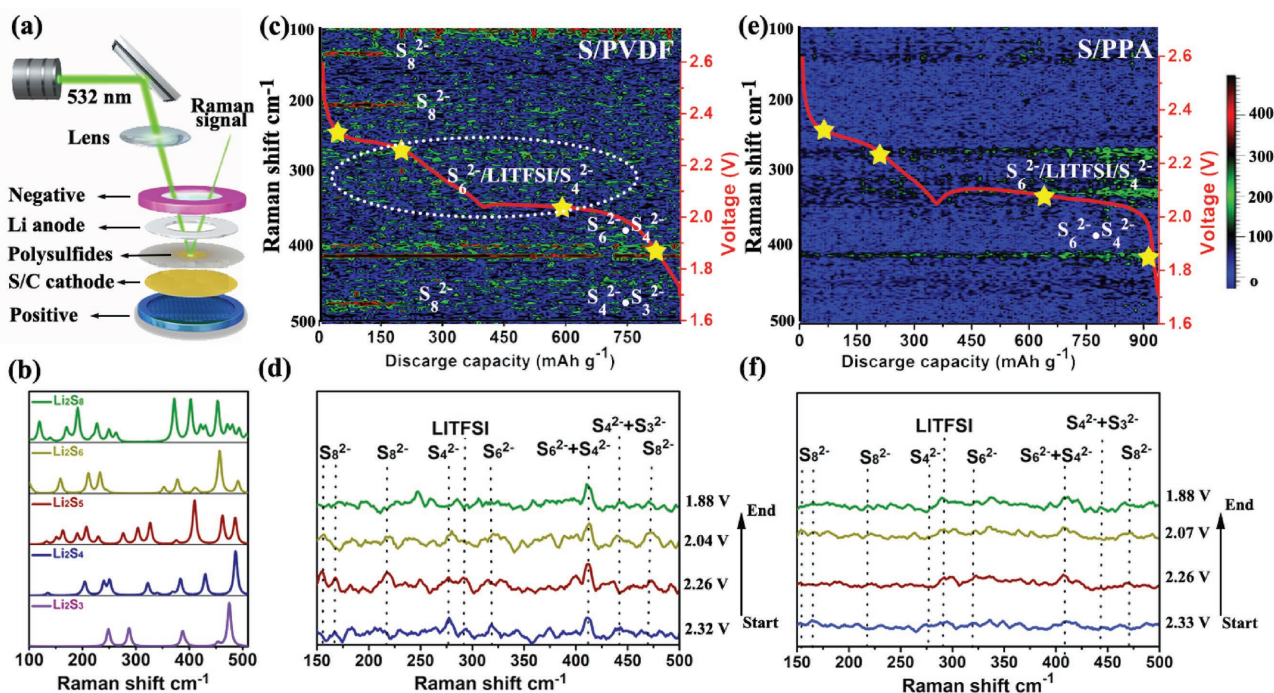


Figure 4. In situ micro-Raman measurements of S/PVDF and S/PPA electrodes during discharging: a) Schematic illustration of Li-S configurations with a sealed glass window for in situ Raman experiments. b) Theoretical (DFT) Raman spectra of polysulfides (Li₂S₃, Li₂S₄, Li₂S₅, Li₂S₆, and Li₂S₈) with a concentration of 20×10^{-3} M. c, e) In situ time-resolved Raman images of the cathode with PVDF and PPA, respectively. d, f) Selected Raman spectroscopy of the cathodes with PVDF and PPA, respectively. The inset red curves in (c) and (e) are voltage profiles of the cathodes with PVDF and PPA, respectively.

Raman spectra (Figure 4b).^[37] In particular, at the first plateau, the peaks intensity of S_8^{2-} anion is strongly highlighted by three characteristic locations at the vicinity of 155, 219, and 478 cm^{-1} , indicating the abundant Li_2S_8 is released from sulfur cathode with PVDF binder.^[37] With the continuous discharge, the signal of S_8^{2-} anion gradually disappears, but the peaks at 324 and 416 cm^{-1} appear, which are attributed to the long-chain and mid-chain polysulfides Li_2S_6 or their mixtures.^[36] Especially, the peaks of Li_2S_6 and Li_2S_4 reach the maximum values when the voltage decreases to the beginning of the second plateau (≈ 2.03 V), implying the change of Li_2S_6 to Li_2S_4 . At the end of the discharge process, the characteristic peaks of Li_2S_4 and Li_2S_3 are located at ≈ 470 cm^{-1} ,^[36] indicating that the soluble mid-chain polysulfides are produced during the second plateau. Observably, serious shuttle effect occurs for the PVDF binder. In contrast, in situ Raman spectra of the cathode with PPA binder are shown in Figure 4e,f. We could clearly observe that no Raman signals of S_8^{2-} are highlighted on the time-resolved Raman image of the PPA binder. At 2.07 V, some highlight bars appear (Figure 4e), which are attributed to Li_2S_6 or Li_2S_4 . Apparently, the PPA binder exhibits stronger capability of absorbing polysulfides than PVDF binder, which verifies the superior performance of the sulfur cathode with polar PPA binder.

To better understand the effect of the chemical/physical characteristic among electrode components, the surface morphology of S/C electrodes with PPA and PVDF binders is characterized using scanning electron microscopy (SEM) and XPS to examine the stability of the electrode before and after galvanostatic cycles (Figure 5). At the macroscopic scale, significant differences can be clearly observed before cycling. The PPA binder presents a uniformly coated electrode in Figure S13 (Supporting Information), exhibiting smooth and uniform structure. In particular, the binder “bridges” emerge between

the adjacent S/C materials (Figure S13b, red arrows, Supporting Information), indicating that the PPA binder has sufficient capacity to connect the active materials. Furthermore, the energy dispersive spectrometer (EDS) mappings of N element (white elliptical circle), as presented in Figure S14b (Supporting Information), further reply that the extremely smooth surface (white elliptical circle) is caused by PPA binder. In addition, the coated film has a strong adhesion to the Al foil. No materials peel off during the subsequent operations after the electrode is repeatedly bended and folded (Figure S15, Supporting Information). There are no swelling and structure changes of S/C/PPA mixtures, implying the PPA polymer binder has very good stability (Figure S16, Supporting Information).

To quantitatively evaluate and compare the mechanical properties of S electrodes with PPA binder, widely adopted peeling tests are employed. As shown in Figure S17 (Supporting Information), the PPA binder shows higher initial peeling stress (≈ 0.46 Mpa), which is about 7.7 times than the reference PVDF binder (≈ 0.06 Mpa). Moreover, few S/C materials with PPA binder could be peeled off from the aluminum foil, which should be observed in the inside digital photographs. The adhesion test clearly indicates that the robust PPA binder contributes to adapt the mechanical strength and maintain structure integrity of S electrodes. With 50 deep galvanostatic discharge at 0.5 C, the S/C/PPA cathode exhibits more uniform structure (Figure 5a) with integral SEI formation after the lithiation. The difference between the samples, however, becomes evident after 50 cycles. The S/C/PVDF cathode shows cracks (Figure 5b, red arrows) over the entire area of the film due to the volume expansion of the S cathode. Therefore, the PPA binder is better at preserving the original film morphology due to the improved multidimensional binding capability based on the hyper-branched polymeric network compared with single-structure

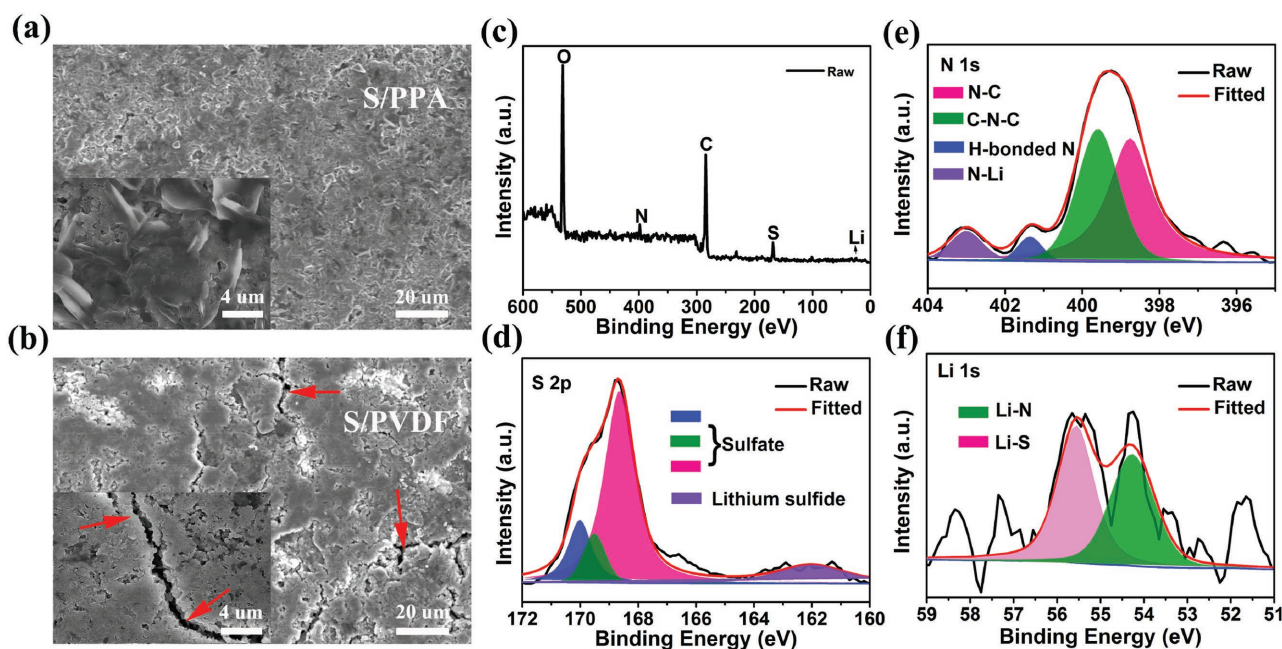


Figure 5. SEM images of sulfur cathodes with a) PPA binder and b) PVDF binder after 50 cycles, respectively. XPS characterization of chemical bonds between PPA binder and sulfur cathodes after discharge, c) wide spectral scan, and d–f) high-resolution spectra of N 1s, S 2p, and Li 1s, respectively.

PVDF binder. These results clearly demonstrate that the 3D crosslinked PPA binder can maintain the electrical and mechanical integrity upon deep galvanostatic cycling. Besides excellent mechanical performance of PPA binder, the bonding between the PPA binder and the polysulfides is further verified by the XPS spectra of the discharge product (Figure 5c). Weak N1s spectrum is observed, but the strong N-Li peak at 403.2 eV is found (Figure 5d), which verifies the strong interaction between the PPA moieties and discharge products. This result is in good agreement with the DFT calculation results (Figure 2g). In the S 2p signal (Figure 5e), lithium sulfide peaks are observed at the neighborhood of 162 eV,^[38,39] indicating the full discharge of elemental sulfur. There is also a sulfate signal resulting from the S–O bond between PPA binder and S (Figure 2g) or from the air and moisture sensitivity of Li₂S. The Li 1s spectrum shows the Li–N and the Li–S signals (Figure 5f), indicating again the strong interactions between cathode discharge polysulfide products and PPA binder. Those benefits of PPA binder are further demonstrated by resolving Li anodes, as shown in Figure S18a (Supporting Information), that a more dense and uniform SEI film can be observed compared with PVDF binder (Figure S18b, Supporting Information). Moreover, less S element on the surface of Li anode is observed, demonstrating the PPA binder can effectively suppress polysulfides shuttling during cycles.^[40] All these results provide direct insight into the mechanism for PPA binder to confine polysulfide species within the cathode.

In summary, we have proposed a new hydrophilic binder with strong polarity and viscosity for anchoring polysulfides for high-energy Li-S batteries. The novel PPA binder exhibits abundant Li–N, Li–O, and S–O bonds, which leads to significant improvements in both cycle retention and rate performance as compared with conventional PVDF binder. With DFT analysis and in situ Raman spectra measurements, we further confirm the origin for the performance enhancement by the strong covalent bonding of polysulfides with PPA binder. The advantages of the PPA binder can be summarized as follows: (i) polar sites of the cross-linked PPA binder effectively ensure strong adhesion of polar discharge products on the S cathode; (ii) the chemical interaction of S–O bond facilitates S immobilization on nonpolar carbon surface for better ion kinetics; and (iii) the excellent mechanical behavior improves the electrode integrity. We believe the currently reported binder represents a major advance in lithium-sulfur battery toward real-life commercial applications.

Experimental Section

Synthesis of the Hydrophilic PPA Binder: Polyethylenimine, ethylenediamine (PEI), and *N,N*-dimethylformamide (DMF) were purchased from Aladdin. PEGDGE was purchased from Sigma-Aldrich; all targets were used as received. To obtain and compare the hydrophilic PPA binders with different cross-linking degrees, different molar ratios of PEGDGE and PEI according to the scheduled molar fractions (typical, 1:2; 1:1; and 1.5:1) of epoxy groups in PEGDGE and amine groups in PEI were copolymerized in DMF solvent with magnetic stirring for 4 h at 140 °C under the N₂ environment. Then different cross-linking degrees of PPA binders were uniformly gained with the lightly yellow product in the DMF solution after cooling to room temperature.

Characterization: FTIR (USA) and XPS (Kratos Axis Ultra Dld, Japan) were used for elemental analysis and possible chemical bonding information. For the adhesion tests, the mixtures of acetylene black and PPA binder were uniformly mixed. The morphology and microstructure of cathode before and after cycles were investigated with SEM on HITACHI SU8010 Japan.

Preparation of S/PPA Cathodes and Electrochemical Measurement: Commercial sulfur powder and acetylene black with a mass ratio of 6:4 were taken and ball-milled for 60 min at 300 rpm. The obtained mixture was then heated at 155 °C for 12 h to encapsulate sulfur in the acetylene black. After cooling to room temperature, the S/C composite was obtained. Then the electrodes were prepared by making slurry of S/C and binder (PPA or PVDF) in a mass ratio of 8:1:1 in DMF solvent. Typically, each electrode contained ≈1.2–1.5 mg of active materials per cm².

The electrolyte was 1 M LiTFSI in a mixture of 1,3-dioxolane (DOL) and 1,2-dimethoxyethane (1:1 v/v) with 1 wt% lithium nitrate (LiNO₃) as additive. Cells were assembled in an argon-filled glove box. For each cell, 35 μL electrolyte was strictly controlled for performance evaluation with various sulfur loading densities. The cyclic voltammetry was tested on CT2001A cell test instrument (Wuhan LAND Electronic Co., Ltd) and CHI660E (Shanghai Chenhua instrument Co., Ltd) electrochemical workstation, respectively.

In Situ Raman Spectroscopy: Li-S coin cells with a quartz window on negative shell were used for in situ micro-Raman spectroscopy analysis. The same method was used to prepare S/PVDF and S/PPA cathodes as aforementioned. A hole was created on lithium metal foil to allow the laser shed on the separator. The cells were run at a charging rate of 0.5 C. Raman signals were recorded simultaneously by a 532 nm laser with an ≈1 μm laser spot on the separators near the lithium ring.

Calculation Method: The atomic configurations and adsorption energies between the binder molecule and Li₂S were calculated by using DFT within the Perdew–Burke–Ernzerhof generalized gradient approximation, as implemented in the Dmol3 package. The double numerical plus polarization basis sets with effective core potential were employed to describe atomic potentials. Self-consistent field calculations (SCF) were carried out until the SCF tolerance was below 1 × 10⁻⁶. The adsorption energy was obtained by subtracting the SCF energies of both Li₂S and binder molecule from the energy of the optimized configuration of Li₂S coordinated to the binder molecule. The HOMO and LUMO of the binder molecule were calculated by DFT simulation at the B#LYP/6-31G* level carried out with the Gaussian 09 package.

The theoretical threshold energy level of binders for cathodes was calculated by the equation: $E_{(eV)} = -4.5 - E_{(NHE)}$ where the normal hydrogen electrode ($E_{(NHE)}$) is the difference between the theoretically highest voltage of cathodes and the lowest redox potential of lithium anode (-3.04 V vs the standard hydrogen potential electrode). For instance, the working potential window of S cathodes lies between 1.5 and 3 V versus Li⁺/Li, which is equivalent to the energy level from -4.46 to -2.96 eV. The energy range between HOMO level and LUMO level of the binders should cover the cathode working energy level; otherwise, the binders will be electrochemically instable in the sulfur cathodes.

The Raman spectra of polysulfides were calculated by DFT simulations at the apdf/6-311G (2d) level carried out with the Gaussian 09 package. The ground state geometries of polysulfides optimized under the same conditions were used to predict Raman peaks, and a uniform scaling factor was set to be 0.965. The universal solvation model was employed to describe the solvent effect of DOL electrolyte in the Li-S battery system.

Supporting Information

Supporting Information is available from the Wiley Online Library or from the author.

Acknowledgements

W.C., T.L., and T.Q. contributed equally to this work. The authors acknowledge support from the National Natural Science Foundation of China (Grant Nos. 51722204, 91421110, 51622208, and 51402202), the National Key Basic Research Program of China (Grant No. 2014CB931702), the Fundamental Research Funds for the Central University (Grant No. ZYGX2016Z004), and the Priority Academic Program Development of Jiangsu Higher Education Institutions (PAPD).

Conflict of Interest

The authors declare no conflict of interest.

Keywords

binders, lithium-sulfur batteries, polysulfides

Received: October 17, 2017
Published online:

- [1] Y. K. Jeong, T. Kwon, I. Lee, T. S. Kim, A. Coskun, J. W. Choi, *Nano Lett.* **2014**, *14*, 864.
- [2] H. Wu, G. Yu, L. Pan, N. Liu, M. T. McDowell, Z. Bao, Y. Cui, *Nat. Commun.* **2013**, *4*, 1.
- [3] X. Tao, J. Wang, C. Liu, H. Wang, H. Yao, G. Zheng, Z. W. Seh, Q. Cai, W. Li, G. Zhou, C. Zu, Y. Cui, *Nat. Commun.* **2016**, *7*, 11203.
- [4] T. Lei, W. Chen, J. Huang, C. Yan, H. Sun, C. Wang, W. Zhang, Y. Li, J. Xiong, *Adv. Energy Mater.* **2016**, *7*, 1601843.
- [5] Q. Pang, X. Liang, C. Y. Kwok, L. F. Nazar, *Nat. Energy* **2016**, *1*, 16132.
- [6] X. L. Ji, L. F. Nazar, *J. Mater. Chem.* **2010**, *20*, 9821.
- [7] G. He, X. L. Ji, L. F. Nazar, *Energy Environ. Sci.* **2011**, *4*, 2878.
- [8] Y. Jiao, W. Chen, T. Lei, L. Dai, B. Chen, C. Wu, J. Xiong, *Nanoscale Res. Lett.* **2017**, *12*, 195.
- [9] R. Xu, J. Lu, K. Amine, *Adv. Energy Mater.* **2015**, *5*, 1500408.
- [10] J. Yang, J. Xie, X. Zhou, Y. Zou, J. Tang, S. Wang, F. Chen, L. Wang, *J. Phys. Chem. C* **2014**, *118*, 1800.
- [11] G. Zhou, Y. Zhao, A. Manthiram, *Adv. Energy Mater.* **2015**, *5*, 1402263.
- [12] J. Song, Z. Yu, M. L. Gordin, D. Wang, *Nano Lett.* **2016**, *16*, 864.
- [13] Z. Zhang, L. L. Kong, S. Liu, G. R. Li, X. P. Gao, *Adv. Energy Mater.* **2017**, *7*, 1602534.
- [14] H. S. Kang, Y. K. Sun, *Adv. Funct. Mater.* **2016**, *26*, 1225.
- [15] T. Lei, Y. Xie, X. Wang, S. Miao, J. Xiong, C. Yan, *Small* **2017**, *13*, 1701013.
- [16] J. Y. Hwang, H. M. Kim, S. K. Lee, J. H. Lee, A. Abouimrane, M. A. Khaleel, L. Belharouak, A. Manthiram, Y. K. Sun, *Adv. Energy Mater.* **2016**, *6*, 1501480.
- [17] G. Zhou, H. Tian, Y. Jin, X. Tao, B. Liu, R. Zhang, Z. W. Seh, D. Zhuo, Y. Liu, J. Sun, J. Zhao, C. Zu, D. S. Wu, Q. Zhang, Y. Cui, *Proc. Natl. Acad. Sci. USA* **2017**, *114*, 840.
- [18] H. J. Peng, D. W. Wang, J. Q. Huang, X. B. Cheng, Z. Yuan, F. Wei, Q. Zhang, *Adv. Sci.* **2016**, *3*, 1500268.
- [19] J. Sun, Y. Sun, M. Pasta, G. Zhou, Y. Li, W. Liu, F. Xiong, Y. Cui, *Adv. Mater.* **2016**, *28*, 9797.
- [20] M. H. Braga, N. S. Grundish, A. J. Murchison, J. B. Goodenough, *Energy Environ. Sci.* **2017**, *10*, 331.
- [21] X. Yao, D. Liu, C. Wang, P. Long, G. Peng, Y. S. Hu, H. Li, L. Chen, X. Xu, *Nano Lett.* **2016**, *16*, 7148.
- [22] A. Manthiram, X. Yu, S. Wang, *Nat. Rev. Mater.* **2017**, *2*, 16103.
- [23] C. Marino, L. Boulet, P. Gaveau, B. Fraisse, L. Monconduit, *J. Mater. Chem.* **2012**, *22*, 22713.
- [24] C. Marino, A. Debenedetti, B. Fraisse, F. Favier, L. Monconduit, *Electrochem. Commun.* **2011**, *13*, 346.
- [25] S. Komaba, N. Yabuuchi, T. Ozeki, Z.-J. Han, K. Shimomura, H. Yui, Y. Katayama, T. Miura, *J. Phys. Chem. C* **2012**, *116*, 1380.
- [26] G. Li, M. Ling, Y. Ye, Z. Li, J. Guo, Y. Yao, J. Zhu, Z. Lin, S. Zhang, *Adv. Energy Mater.* **2015**, *5*, 1500878.
- [27] P. Bhattacharya, M. I. Nandasiri, D. Lv, A. M. Schwarz, J. T. Darsell, W. A. Henderson, D. A. Tomalia, J. Liu, J. Zhang, J. Xiao, *Nano Energy* **2016**, *19*, 176.
- [28] M. J. Lacey, F. Jeschull, K. Edström, D. Brandell, *J. Power Sources* **2014**, *264*, 8.
- [29] J. Wang, Z. Yao, C. W. Monroe, J. Yang, Y. Nuli, *Adv. Funct. Mater.* **2013**, *23*, 1194.
- [30] W. Chen, T. Qian, J. Xiong, N. Xu, X. Liu, J. Liu, J. Zhou, X. Shen, T. Yang, Y. Chen, C. Yan, *Adv. Mater.* **2017**, *29*, 1605160.
- [31] S. Quan, S. Li, Z. Wang, X. Yan, Z. Guo, L. Shao, *J. Mater. Chem. A* **2015**, *3*, 13758.
- [32] W. Wang, X. D. Liu, Y. B. Xie, H. A. Zhang, W. T. Yu, Y. Xiong, W. Y. Xie, X. J. Ma, *J. Mater. Chem.* **2006**, *16*, 3252.
- [33] G. Xu, Q. B. Yan, A. Kushima, X. Zhang, J. Pan, J. Li, *Nano Energy* **2017**, *31*, 568.
- [34] B. Zhang, X. Qin, G. R. Li, X. P. Gao, *Energy Environ. Sci.* **2010**, *3*, 1531.
- [35] C. Y. Du, C. H. Gao, G. P. Yin, M. Chen, L. Wang, *Energy Environ. Sci.* **2011**, *4*, 1037.
- [36] M. Hagen, P. Schiffels, M. Hammer, S. Dörfler, J. Tübke, M. J. Hoffmann, S. Kaskel, *J. Electrochem. Soc.* **2013**, *160*, A1205.
- [37] J. J. Chen, R. M. Yuan, J. M. Feng, Q. Zhang, J. X. Huang, G. Fu, M. Zheng, B. Rin, Q. F. Dong, *Chem. Mater.* **2015**, *27*, 2048.
- [38] Z. Wang, Y. Dong, H. Li, Z. Zhao, H. B. Wu, C. Hao, S. Liu, J. Qiu, X. W. Lou, *Nat. Commun.* **2014**, *5*, 5002.
- [39] L. Ma, H. L. Zhuang, S. Wei, K. E. Hendrickson, M. S. Kim, G. Cohn, R. G. Henning, L. A. Archer, *ACS Nano* **2015**, *10*, 1050.
- [40] N. Xu, T. Qian, X. Liu, J. Liu, Y. Chen, C. Yan, *Nano Lett.* **2017**, *17*, 538.